Biochemistry

pubs.acs.org/biochemistry Article

Population Distributions from Native Mass Spectrometry Titrations Reveal Nearest-Neighbor Cooperativity in the Ring-Shaped Oligomeric Protein TRAP

Melody L. Holmquist, Elihu C. Ihms, Paul Gollnick, Vicki H. Wysocki,* and Mark P. Foster*

Cite This: https://dx.doi.org/10.1021/acs.biochem.0c00352 Read Online

ACCESS | Metrics & More | Article Recommendations | Supporting Information

ABSTRACT: Allostery pervades macromolecular function and drives cooperative binding of ligands to macromolecules. To decipher the mechanisms of cooperative ligand binding, it is necessary to define, at a microscopic level, the thermodynamic consequences of binding of each ligand to its energetically coupled site(s). However, extracting these microscopic constants is difficult for macromolecules with more than two binding sites, because the observable [e.g., nuclear magnetic resonance (NMR) chemical shift changes, fluorescence, and enthalpy] can be altered by allostery, thereby distorting its proportionality to site occupancy. Native mass spectrometry (MS) can directly quantify the populations of homo-oligomeric protein species with different numbers of bound ligands, provided the populations are proportional to ion counts and that MS-compatible electrolytes do not alter the overall thermodynamics. These measurements can help decipher allosteric mechanisms by providing unparalleled access to the statistical thermodynamic partition function. We used native MS (nMS) to study the cooperative binding of tryptophan (Trp) to *Bacillus stearothermophilus trp* RNA binding attenuation protein (TRAP), a ring-shaped homo-oligomeric protein complex with 11 identical binding sites. MS-compatible solutions did not significantly perturb protein structure or thermodynamics as assessed by isothermal titration calorimetry and NMR spectroscopy. Populations of Trp_n-$TRAP_{11}$ states were quantified as a function of Trp concentration by nMS. The population distributions could not be explained by a noncooperative binding model but were described well by a mechanistic nearest-neighbor cooperative model. Nonlinear least-squares fitting yielded microscopic thermodynamic constants that define the interactions between neighboring binding sites. This approach may be applied to quantify thermodynamic cooperativity in other ring-shaped proteins.

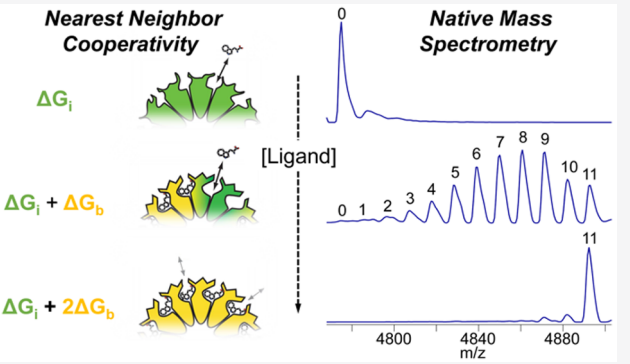

Allosteric communication between ligand binding sites in homo-oligomeric proteins provides a powerful means of regulating their function.[1−3] Even for the best characterized homo-oligomeric allosteric proteins, like hemoglobin, the AAA + proteases,[4] and GroES/GroEL chaperonins,[5,6] the mechanisms of allosteric communication remain controversial and poorly understood, or described only phenomenologically. Cooperativity is most commonly diagnosed from ligand binding curves that fit poorly to a simple Langmuir isotherm. Sigmoidal curves arising from positive cooperativity can be diagnostic; fitting such data with the Hill equation can provide a numerical descriptor of the steepness of the binding curve. However, the Hill coefficient is phenomenological, cannot be interpreted thermodynamically without further assumptions, and has limited mechanistic value.[7] To decipher the mechanisms that lead to positive or negative cooperativity in ligand binding, it is necessary to quantify the microscopic thermodynamic linkages between allosteric sites and the resulting shifts in populations of protein−ligand states.[8−12]

Mechanistic modeling can provide access to microscopic thermodynamic parameters, but the lack of proportionality between experimental observables and the liganded state of a cooperative binding lattice complicates thermodynamic analysis. Isothermal titration calorimetry (ITC) is generally the method of choice for characterizing binding thermodynamics, with some important examples of its utility in studying cooperative interactions.[13−15] ITC directly measures the change in enthalpy (ΔH) resulting from binding of a ligand to a macromolecule; fitting the data to an appropriate binding model yields the overall free energy change ΔG via the equilibrium association constant K_A. However, cooperativity can alter each of these thermodynamic parameters, because

Received: April 27, 2020
Revised: June 18, 2020
Published: June 19, 2020

binding of successive ligands may occur with a higher or lower affinity and be more or less enthalpic, and it becomes difficult to disentangle the thermodynamics of overlapping and simultaneous binding events.[12,16] Moreover, under conditions with high c values, defined as the ratio between the concentration of the binding sites to the equilibrium dissociation constant,[17] cooperative effects can be easily masked.[12,16] These complications make it difficult to determine the populations of various liganded states through the course of a titration and thus to quantify their relative free energies.

Native mass spectrometry (nMS)[18,19] has the potential to resolve the problem of quantifying liganded populations in oligomeric proteins.[20,21] Unlike unidimensional metrics like heat, fluorescence intensity, or chemical shift, wherein it might be difficult to discern whether half of the sites on each oligomer are bound, or half of the oligomers are fully bound, the number of bound ligands can be directly read out from the masses of the species. Provided the binding of individual ligands can be resolved under the given experimental conditions, and that the detected signals are proportional to the states present in solution, native MS can provide unparalleled detail about the populations of accessible ligand−macromolecule states, and therefore the statistical thermodynamic partition function, including microscopic thermodynamic cooperativity parameters.[21,22]

Under "soft" ionization conditions, nMS preserves the tertiary and quaternary structures of protein complexes, allowing investigation of the stability, conformation, topology, interactions, and stoichiometry of their subunits.[18,19] In nMS, nanoelectrospray ionization is used to produce multiply protonated protein complexes, comprising a narrow range of charge states, while retaining much of their native tertiary structures in the gas phase. Due to the deleterious effects of classic biochemical solutions such as potassium phosphate, Tris, and HEPES, macromolecule samples are sprayed from solutions comprising volatile electrolytes, such as ammonium bicarbonate, ammonium acetate (AmAc), or ethylenediamine diacetate (EDDA).[23−25] While various gas-phase evidence suggests that protein tertiary and quaternary structures are retained when sprayed from these solutions,[26−28] effects of MS electrolytes on solution structures and ligand binding affinities remain poorly understood. In the literature, there is a disparity in the solution experiments with MS electrolytes.

We examined the utility of nMS for quantifying populations of liganded states of the oligomeric tryptophan binding protein TRAP from *Bacillus stearothermophilus* (*Bst*) and for determining microscopic thermodynamic parameters describing its homotropic cooperativity. The *trp* RNA binding attenuation protein (TRAP) is a paradigmatic RNA binding gene regulatory protein that controls both transcription and translation of genes involved in tryptophan metabolism in numerous Gram-positive bacteria.[29] *Bst* TRAP is a small 74-residue protein that oligomerizes via intermolecular β sheets to form a circular homo-oligomeric structure composed of 11 subunits that can bind up to 11 Trp ligands in sites located between adjacent subunits (Figure 1). Tryptophan binding activates TRAP to bind to a specific RNA sequence located upstream of the *trp* operon, whereas in the absence of Trp, the protein remains oligomeric but RNA binding is disfavored. Short loops that form part of each binding site, and structurally connect adjacent sites, are highly dynamic in the absence of Trp and become ordered upon binding of individual Trp ligands.[30−33] The ligand-induced structural coupling between adjacent sites provides a unique opportunity to study mechanisms of homotropic cooperativity in protein−ligand binding.

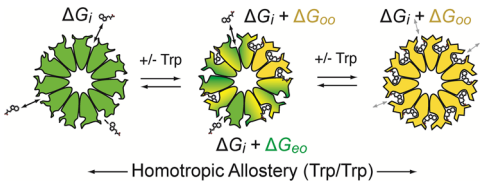

Figure 1. Tryptophan (Trp) binding to the homoundecameric (11-mer) ring protein TRAP and nearest-neighbor (NN) microscopic free energy terms to describe cooperative Trp binding. Inactive apo $TRAP_{11}$ (green) binds up to 11 Trp residues in identical sites located between adjacent protomers. Trp binding results in local conformational changes to each protomer that activate the ring for binding specific sequences in the *trp* leader RNA (yellow). Each binding event induces conformational changes in protomers on both sides of each site (green-yellow). The NN model posits an intrinsic free energy ΔG_i for Trp binding to sites with no occupied neighbors, whereas binding to sites with one or two occupied neighbors incurs additional free energy terms ΔG_{oe} and $2\Delta G_{oo}$, respectively; non-neighboring sites do not contribute. The NN terms quantify the allosteric communication between sites.

Allostery in TRAP has been the subject of numerous past studies that often yielded conflicting results and fell short of detailed mechanistic insight.[29,31,34−39] Equilibrium dialysis experiments of Trp binding with TRAP from *Bacillus subtilis* yielded apparent binding constants of 5−10 μM, and weak cooperativity via Hill coefficients of 1.5−2.[39,40] Weak or no cooperativity was found via Hill analysis[37] or single-temperature ITC studies of *B. stearothermophilus* TRAP at high c values.[31] In contrast, at lower concentrations, and at different temperatures, multiple-mode thermodynamic binding could be discerned.[12] The application of mechanism-based statistical thermodynamic modeling yielded good fits to a nearest-neighbor circular lattice model, indicating weak thermodynamic coupling of ∼1 kcal mol^{-1} between sites. Nevertheless, the large number of parameters involved in fitting NN models to ITC data compels additional model validation.

Because *Bst* TRAP retains its quaternary structure in the gas phase,[41−43] we explored the use of nMS for quantifying cooperativity in Trp binding to *Bst* TRAP. We used heteronuclear NMR and ITC to examine the effect of the MS-compatible solutions of AmAc and EDDA on the structure and thermodynamics of Trp binding by *Bst* TRAP, compared charge states and ligand populations of ions in ESI-MS generated from EDDA and AmAc solutions, examined the charge state dependence of liganded populations, measured ligand-dependent population shifts during replicate titrations, and compared ensemble population shifts (fractional saturation) with similar solution measurements. Nonlinear least-squares fitting of nMS experimental and best fit distributions of Trp_n-$TRAP_{11}$ states from noncooperative and nearest-neighbor (NN) cooperative models rules out site independence and yielded good agreement with modest nearest-neighbor cooperativity previously reported from temperature-dependent ITC data.[12] Considering the cyclic structure of TRAP and intimate contact between neighboring protomers, NN models posit that binding of a ligand to a site alters the free energy change of neighboring sites upon binding their ligands (i.e., their affinity). Quantifying this microscopy energy transduction

https://dx.doi.org/10.1021/acs.biochem.0c00352
Biochemistry XXXX, XXX, XXX−XXX

thus provides an important step toward understanding the structure−thermodynamic links that lead to cooperative ligand binding in proteins.

MATERIALS AND METHODS

Expression and Purification of *Bst* TRAP. TRAP was expressed in *Escherichia coli* BL21(DE3) cells and purified by ion exchange chromatography followed by denaturation with 6 M guanidinium hydrochloride (GdnHCl) and purification by reverse-phase high-performance liquid chromatography to ensure removal of bound Trp, as described previously.[30] Purified, lyophilized protein was dissolved in 6 M guanidinium hydrochloride (GdnHCl), 50 mM sodium phosphate, and 100 mM NaCl (pH 8) and refolded by a stepwise dialysis against 3 M, 1.5 M, and 0 M denaturant. Except where indicated, TRAP concentrations are specified with respect to a protomer (i.e., 11[$TRAP_{11}$]).

NMR. Purified, refolded [U-^{15}N]-apo TRAP was divided into three 600 μL aliquots with the concentration of TRAP for each aliquot ranging from 1.3 to 1.4 mM and dialyzed into 50 mM $NaPO_4$ and 100 mM NaCl (pH 8.0), 100 mM ammonium acetate (pH 8.0), and 100 mM ethylenediamine diacetate (pH 8.0) buffers using 0.5 mL dialysis cassettes with a 3.5 kDa molecular weight cutoff (Thermo Slide-A-Lyzer, catalog no. 66333) at 4 °C, with gentle stirring. The pH of the phosphate solution was adjusted with 3 M NaOH. The pHs of the AmAc and EDDA solutions were adjusted with 10% ammonium hydroxide. Each NMR sample contained ∼1 mM TRAP protomers as measured by the Bradford assay with the Coomassie Plus Bradford reagent and bovine serum albumin as the standard. Two-dimensional ^{15}N−^{1}H TROSY-HSQC spectra were recorded at 55 °C on a Bruker Avance III HD 800 MHz spectrometer equipped with a 5 mm (TXI) cryoprobe with *Z*-axis gradients, with 64 time points and a 40 ppm spectral width in the ^{15}N dimension.

ITC. Aliquots of 10 mL of 100 μM purified, refolded apo-TRAP were dialyzed against 1 L each of three NMR buffers mentioned above for 12 h at 4 °C, and 1 mM Trp stock solutions were prepared from the dialysates. For ITC experiments, a MicroCal VP-ITC isothermal titration calorimeter (Malvern Panalytical) was used. For the final concentrations, Trp and TRAP were diluted with the dialysate solutions to 600 μM Trp in the syringe and 60 μM TRAP in the cell. Titrations were performed at 25 °C, using an initial 3 μL injection followed by 50 injections of 5 μL, with a delay of 200 s between injections. Data were fit to a single-site model with a single apparent K_A using Origin 7.0 (OriginLab).

Native Mass Spectrometry. Aliquots of purified and refolded *Bst* TRAP in phosphate buffer were exchanged twice into 200 mM ethylenediamine diacetate (EDDA; Sigma-Aldrich, catalog no. 420352) or 400 mM ammonium acetate (AmAc; Sigma-Aldrich, catalog no. 431311) using a P-6 Micro Bio-Spin (Bio-Rad) column. The concentration of TRAP was determined with a Nanodrop 2000c spectrophotometer (Thermo Scientific) using a monomer absorbance at 280 nm of 2980 M^{-1} cm^{-1} and a mass of 8242.6 Da.[33] Trp stock solutions (10 mM) were prepared by dissolution in the same solutions used for TRAP and filtered with a 0.22 μm filter. Trp stocks were diluted to 1 mM, 750 μM, and 500 μM for native MS titration experiments. Concentrations of Trp stocks were determined with a Nanodrop 2000c spectrophotometer using an extinction coefficient at 280 nm of 5690 M^{-1} cm^{-1} and a mass of 204.2 Da.[44] Native mass spectra were recorded on an Exactive EMR Plus Orbitrap column (Thermo) modified in house with a custom mass selection quadrupole and a surface-induced dissociation (SID) device (not used in this study).[45] Data were collected at a source temperature of 175 °C, a nanoESI capillary voltage of 0.9−1.1 kV, an in-source CID of 10 V, an HCD of 10 V, and a mass range of m/z 500−14000. Flythrough (transmission) voltages were tuned to minimize activation and loss of Trp; voltages for the source DC offset, injection flatapole, inter flatapole, and bent flatapole were set at 7, 6, 5, and 5 V, respectively. The C-trap bias was −10 V; the resolution was 8750 as defined at m/z 200. A trap gas setting of 4 (arbitrary units) was used to record mass spectra of samples with >11 μM TRAP, and trap gas 8 was used for the samples with <11 μM TRAP for improved signals. Borosilicate glass capillary emitters were pulled in house with a Sutter Flaming/Brown Micropipette puller P97. Native mass spectra were recorded for at least 1 min under each Trp condition with three different emitter tips; triplicates of spectra with TRAP were acquired at 14 Trp concentrations ranging from 0 to 110 μM.

The populations of Trp_n-$TRAP_{11}$ species were determined from integrated peak areas after spectral deconvolution using UniDec.[46] Deconvolution was performed without smoothing, with an m/z range of 3800−5700 (which includes charge states of +21 to +18 for TRAP 11-mers), with a mass range of 91000−110000 Da, with a mass sampling of 10 Da, and with a peak full width at half-maximum of 2.5, in manual mode, with a peak detection range of 3 Da, with a peak threshold of 0.001, and with an integration range of −50 to 50 Da. TRAP peaks were selected by manual assignment and integrated by UniDec. Populations were corrected for small amounts of Trp-loaded TRAP 12-mers by manual assignment and peak area subtraction. Fractional saturation $\overline{Y}$ at each Trp concentration was obtained from the sum of the bound Trp species at each Trp concentration:

$$\overline{Y} = \sum_{i=0}^{11} (iA_i/11)$$

where A_i is the area of peaks corresponding to TRAP with i bound Trp residues. To account for sample losses during buffer exchange, binding site concentrations were corrected by fitting fractional saturation data with an independent sites model $M + L \overset{K_{D,app}}{\longleftrightarrow} ML$ while allowing optimization of the binding site concentration M_t (i.e., 11 times the concentration of $TRAP_{11}$ rings) and apparent dissociation constant $K_{D,app}$. Similar results were obtained by numerical optimization of ordinary differential equations derived from the model[47] or analytically directly using the binding quadratic:

$$\overline{Y} = (K_d + L_t + M_t - \sqrt{(K_d + L_t + M_t)^2 - 4L_tM_t})/2M_t$$

where L_t is the total Trp concentration (Figure S1). The relative abundances of the 12 possible stoichiometries of TRAP and Trp (0−11) at each concentration of TRAP and Trp (Trp_n-$TRAP_{11}$) were fit using *itcsimlib* as previously described[12] with slight modifications. Three statistical thermodynamic models were considered: (I) an independent sites model parametrized by an intrinsic binding free energy ΔG_i, (II) a nearest-neighbor additive model parametrized by an intrinsic free energy change ΔG_i for binding to sites with no occupied neighbors and a cooperativity term ΔG_{nn} that is doubled when both neighboring sites are occupied, and (III) a

https://dx.doi.org/10.1021/acs.biochem.0c00352
Biochemistry XXXX, XXX, XXX−XXX

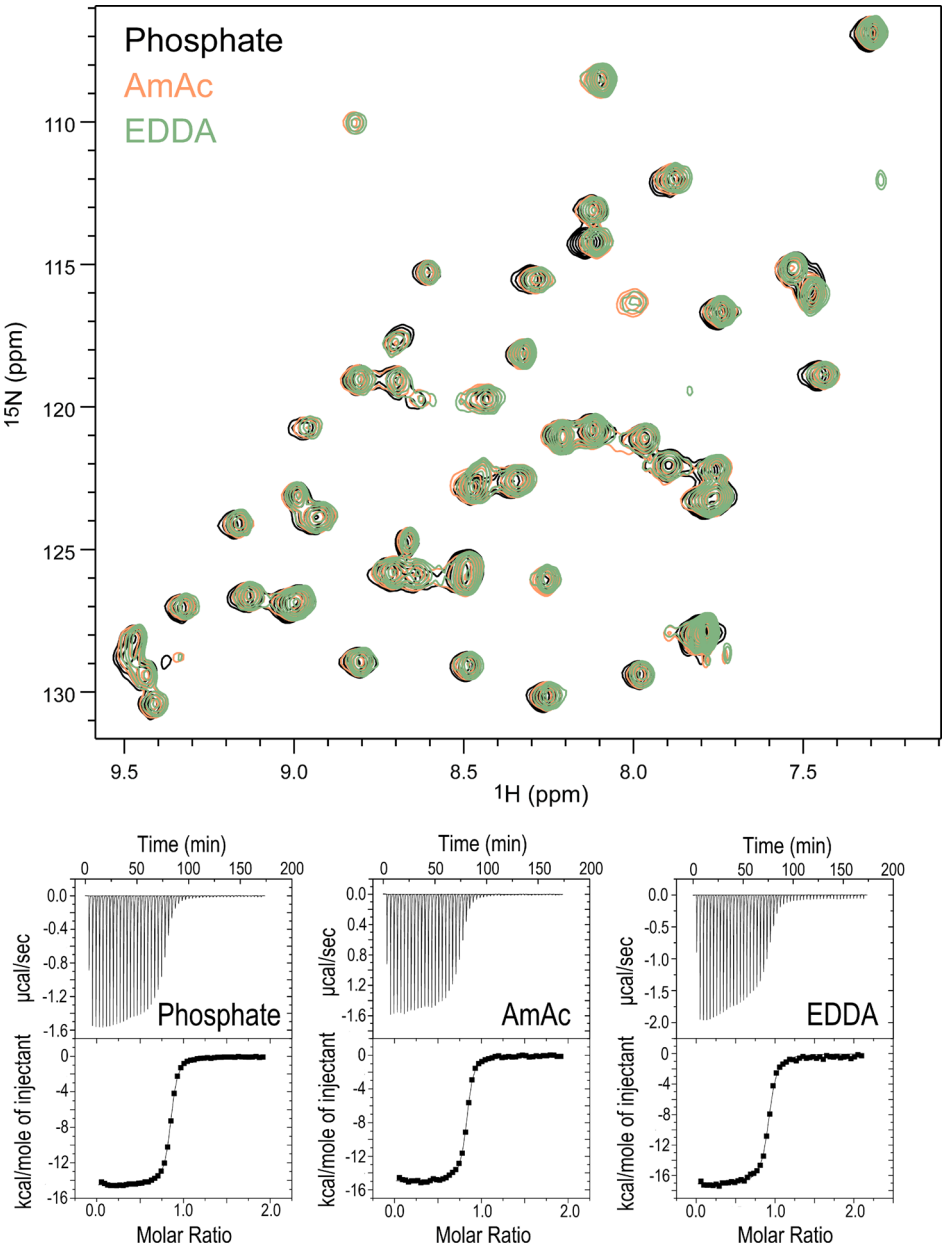

Figure 2. Solutions that are compatible with native mass spectrometry (nMS) do not significantly alter the structure of TRAP or its Trp binding thermodynamics. Two-dimensional $^{15}N-^{1}H$ TROSY-HSQC spectra (top) of 1.3−1.4 mM TRAP recorded at 800 MHz in typical [50 mM sodium phosphate and 100 mM NaCl (pH 8.0)] or nMS-compatible solutions [100 mM ammonium acetate (AmAc) (pH 8.0) or 100 mM ethylenediamine diacetate (EDDA) (pH 8.0)]; most resonances superpose within <0.02 ppm. Isothermal titration calorimetry (ITC) yields similar thermograms (bottom) in phosphate and nMS-compatible solutions. ITC titrations were performed at 25 °C with 600 μM Trp titrated into 60 μM TRAP in (i) 50 mM sodium phosphate and 100 mM NaCl (pH 8.0), (ii) 100 mM ammonium acetate (pH 8.0), and (iii) 100 mM ethylenediamine diacetate (pH 8.0). Apparent dissociation constants fitted to a one-site model were 0.115 ± 0.003, 0.173 ± 0.014, and 0.183 ± 0.010 μM in phosphate, AmAc, and EDDA, respectively.

non-additive model parametrized by ΔG_i and cooperativity terms ΔG_{eo} and ΔG_{oo} that correspond to the effects of having one or two occupied neighbors (Figure 1).[12] Suitable binding polynomials are constructed in an automated manner by *itcsimlib* by iterating over all possible Trp_n-$TRAP_{11}$ configurations (2^{11} = 2048), and statistical thermodynamic probabilities are computed at each ligand and binding site concentration; in comparison to fitting ITC data, populations are used directly, instead of being computed from binding enthalpies. Free energy terms of the model were optimized by numerical minimization of the reduced χ^2 value between the experimental and simulated populations using an estimated variance of 0.05%.

RESULTS AND DISCUSSION

The TRAP Structure Is Unperturbed by MS-Compatible Electrolyte Solutions. To be useful for measuring binding thermodynamics, the conditions used for recording native mass spectra should not perturb the quaternary structure or populations of free and bound states, and the detected ion counts should mirror the abundance of the species present in solution. We used two-dimensional NMR

https://dx.doi.org/10.1021/acs.biochem.0c00352
Biochemistry XXXX, XXX, XXX−XXX

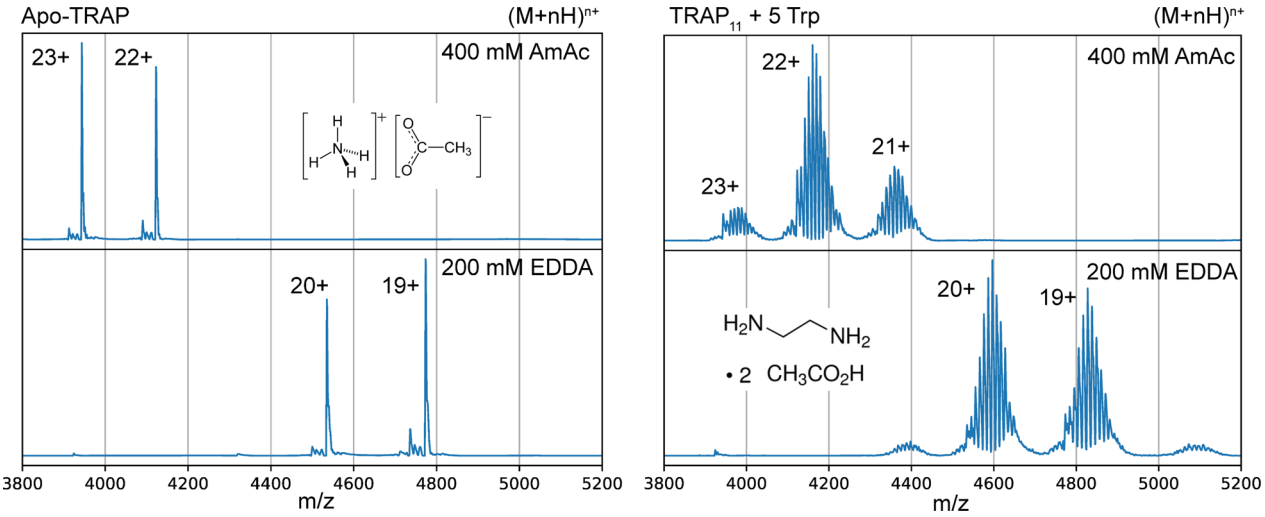

Figure 3. Nano-ESI spectra of TRAP exhibit native-like features, including narrow charge state distributions, an oligomeric state corresponding to a TRAP 11-mer, and noncovalent ligand interactions. Mass spectra were obtained for 5 μM *Bst* $TRAP_{11}$ in 400 mM AmAc and 200 mM EDDA. In the left panels, Trp-free apo-$TRAP_{11}$ exhibits dominant 23+ and 22+ charge states when sprayed from 400 mM AmAc and 20+ and 19+ charge states from 200 mM EDDA. In the right panels, $TRAP_{11}$ in the presence of 25 μM Trp retains similar populations of Trp_n-$TRAP_{11}$ states, with slightly higher charge states (23+ to 21+) in AmAc than in EDDA (21+ to 18+). The chemical structures correspond to AmAc (top left) and EDDA (bottom right).

spectroscopy to examine the effect of MS-compatible solutions on the solution structure of TRAP. Two-dimensional $^{15}N-^{1}H$ TROSY-HSQC spectra of TRAP were recorded in both typical and nMS-compatible pH 8 solutions: (1) 50 mM sodium phosphate and 100 mM NaCl, (2) 100 mM ammonium acetate (AmAc), and (3) 100 mM ethylenediamine diacetate (EDDA) (Figure 2, top). The 11-fold symmetry of the 91 kDa Trp-free TRAP oligomer results in spectra that feature a single set of resonances for each of the amino acids in the 74-residue protein. NMR spectra from each of the solutions exhibited indistinguishable chemical shifts and line widths for nearly all signals observed in the spectra; only three resonances exhibit chemical shift perturbations (CSPs) of >0.02 ppm. While there is evidence for more native-like structure of lower-charge ions sprayed from EDDA versus AmAc,[41,42,48,49] there were no CSPs of >0.02 ppm between those conditions, indicating that the solution structure of TRAP in those buffers is indistinguishable. Likewise, the amide spectra of TRAP in the presence of excess Trp were similarly unperturbed by the choice of the electrolyte solution (Figure S2). As amide chemical shifts are highly sensitive to changes in the local electronic environment, we conclude that the protein structure is not significantly altered by the solution components investigated.

TRAP Binds Trp with Comparable Thermodynamics in MS-Compatible Electrolyte Solutions. We used ITC to test whether use of MS-compatible solutions might alter Trp binding thermodynamics. Identical TRAP samples were dialyzed into each of the solutions used in NMR experiments [phosphate, AmAc, and EDDA (pH 8)] and loaded into the sample cell, while crystalline Trp was dissolved in the corresponding buffers and loaded into the syringe; titration experiments were performed at 25 °C (Figure 2, bottom). Although Trp exhibits weak cooperativity in binding to TRAP (as shown below and previously noted in temperature-dependent studies),[12] thermograms from each solution were reasonably well described by a single-site model. Fitting integrated enthalpies yielded similar binding enthalpies (ΔH values of -14.51 ± 0.02, -16.00 ± 0.05, and -16.92 ± 0.08 kcal mol^{-1}) and affinities ($K_{d,app}$ values of 0.115 ± 0.003, 0.173 ± 0.014, and 0.183 ± 0.010 μM) in phosphate, AmAc, and EDDA solutions, respectively. These affinity differences are within thermal energy (RT = 590 cal/mol at 25 °C), and thus, we conclude that under these conditions the thermodynamics of the Trp−TRAP interaction are not significantly perturbed by the MS-compatible AmAc and EDDA solutions in comparison to the use of phosphate buffer.

The Choice of the Electrolyte Solution Does Not Significantly Affect Measurement of Trp-TRAP Binding by Native MS. Before proceeding to quantitatively interpret populations of Trp_n-$TRAP_{11}$ states in a titration, we examined the possibility that the choice of solution might affect the ion counts in the gas phase. Previous nMS experiments with TRAP have shown that Trp can remain bound to TRAP when the ligand is in excess, and though populations of states were not interpreted quantitatively, different gas-phase structures were inferred from ion mobility experiments.[41,42] To determine the effect of an electrolyte solution on MS-detected charge states and populations of ions corresponding to TRAP complexes with varying numbers of bound Trp, we recorded nMS spectra of TRAP in the absence and presence of Trp from both AmAc and EDDA solutions (Figure 3).

Whether the compounds are sprayed from AmAc or EDDA, spectra in the absence of Trp were dominated by ions corresponding to multiply charged intact undecamers (90665.96 Da). In the EDDA solution (pH 8), the dominant charge state distribution (CSD) includes 20+ and 19+ charge states, while in AmAc (pH 7), we observed a distribution of higher charge states, with dominant 23+ and 22+ charge states; this charge state difference is consistent with previous findings.[41,42,48,49] In the presence of roughly $^{1}/_{2}$ equiv of Trp per binding site (~5.5 equiv per $TRAP_{11}$ ring), we observe for each charge state a series of well-separated peaks that correspond to the mass of $TRAP_{11}$ with varying numbers of bound Trp ligands (from 0 to 11). In either AmAc or EDDA, spectra yielded narrow charge state distributions and well-

https://dx.doi.org/10.1021/acs.biochem.0c00352
Biochemistry XXXX, XXX, XXX−XXX

resolved peaks corresponding to similar distributions of Trp_{0-11}-$TRAP_{11}$ states. Well-resolved peaks of the Trp_n-$TRAP_{11}$ states yielded similar quantification of populations from either intensities or integration of peak areas, consistent with the fact that peak widths and shapes do not vary significantly across the measured m/z range.

Native MS Allows Quantification of Populations of Trp_n-$TRAP_{11}$ States. Solution NMR and ITC experiments showed no significant difference in structure or thermodynamics between phosphate buffer and AmAc and EDDA solutions, so we proceeded with native MS experiments to measure populations of Trp_n-$TRAP_{11}$ states sprayed from 200 mM EDDA solutions (pH 8) after premixing a range of TRAP concentrations with a range of Trp concentrations from 0 to ~2-fold excess relative to the number of binding sites. Over the course of a typical titration (Figure 4), a clear shift in

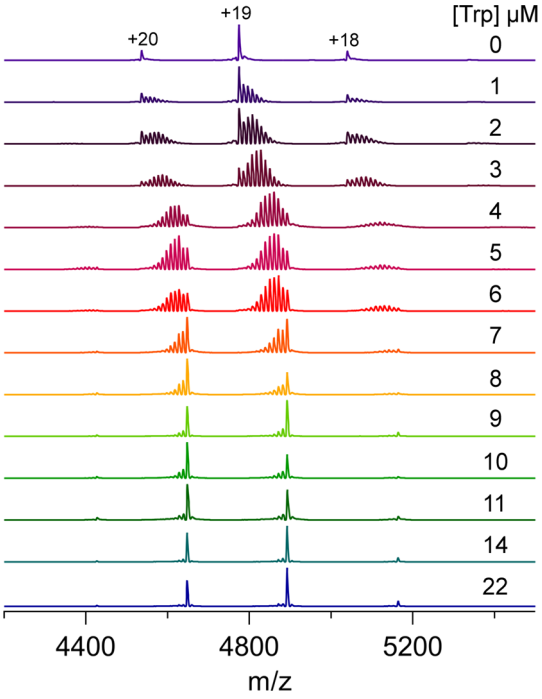

Figure 4. Native MS reveals populations of Trp_n-$TRAP_{11}$ states via a titration. $TRAP_{11}$ (0.5 μM) in EDDA (200 mM) was titrated with 1−22 μM Trp, yielding prominent ions in 20+ to 18+ charge states, with 0−11 bound Trp residues. At 0 μM Trp, only the apo form of $TRAP_{11}$ is observed, whereas at high Trp concentrations, the Trp_{11}-$TRAP_{11}$ signals predominate.

populations is observed, starting from apo-TRAP [Trp_0-$TRAP_{11}$, 90657 Da (top spectrum in Figure 4)] to holo-TRAP [Trp_{11}-$TRAP_{11}$, 92930 Da (bottom spectrum)]. Throughout most of the titration series in EDDA, spectra are dominated by signals from the 20+ and 19+ charge states. For this series, with ~5 μM binding sites, signals from fully bound holo-TRAP (Trp_{11}-$TRAP_{11}$) become the dominant feature of the spectrum above 7 μM Trp (~1.4 equiv), indicating a c value (c = [sites]/K_d = [5.46 μM/0.5 μM]), not far above 1 (see below for $K_{D,app}$).[17] With a low c value, there is a substoichiometric binding of Trp to TRAP under these conditions.

Populations of Trp_n-$TRAP_{11}$ species at each Trp concentration were obtained by integration of deconvoluted spectra (Figure S1). The low extinction coefficient of TRAP (ε_{280} = 2980 M^{-1} cm^{-1})[12] and additional handling steps while performing electrospray experiments made it difficult to precisely control protein concentration. Protein concentrations were corrected by nonlinear least-squares fitting of the summed bound fraction $\bar{Y}$ with an independent sites model (Figure S3). Fits yielded corrected protein concentrations with percent changes ranging from 15.8% to 54.7% from initial TRAP concentrations (Table S1) and apparent dissociation constants $K_{D,app}$ of ~0.5 μM for each Trp binding site (Figure S3 and Table S1). Trp concentrations (ε_{280} = 5690 M^{-1} cm^{-1})[44] were taken to be accurate. Importantly, the resulting populations of Trp_n-$TRAP_{11}$ species allow separate quantitation of $TRAP_{11}$ species with different numbers of bound Trp residues, whereas this information is difficult to obtain from conventional approaches such as ITC, which provide only a measure of overall fractional saturation (Figure S1 and Figure 2, bottom).

Cooperative Trp Binding to $TRAP_{11}$ Is Evident from Population Distributions. Independent quantification of Trp_n-$TRAP_{11}$ populations clearly distinguishes independent and cooperative ligand binding. The unidimensional metric of fractional saturation $\bar{Y}$ could be readily fit by a binding polynomial with a single equilibrium constant (Figure S3 and Table S1), so we first tested whether the experimentally determined Trp_n-$TRAP_{11}$ populations (Figure 5, left, 19+ charge state used for illustration) could be explained by a model with 11 independent sites (i.e., a binomial distribution). To facilitate visual assessment of the fit of the independent sites model, we simulated MS data for individual charge states from populations computed from the best fit parameters for the model (Figure 5, middle). Simulated spectra from the independent sites model were in poor agreement with the experimental data, featuring a generally narrower distribution across the titration range. On the other hand, fitting the experimental populations with binding polynomials generated from a nearest-neighbor model produced broader distributions of Trp_n-$TRAP_{11}$ states and generally good fits to the experimental data (Figure 5, right). This binding model is parametrized with an intrinsic affinity of isolated sites for binding to a Trp ligand, ΔG_i, and terms for how this affinity is altered by the occupancy of one or two neighboring sites, ΔG_{oe} and ΔG_{oo} (Figure 1). Although the average fractional saturation could be readily fit with the independent sites noncooperative model, the stark difference in population distributions generated from the model to those obtained experimentally clearly illustrates the inadequacy of the model. By comparison, the close agreement between the experimental population distributions and those simulated from the nearest-neighbor model illustrates the advantage of being able to independently measure different components of the partition function and highlights the tremendous advantage of using native MS to monitor ligand binding to proteins with multiple binding sites.

Populations derived from native MS spectra of each of the six independent titration experiments were described well by the nearest-neighbor model, allowing quantification of three microscopic free energy terms, ΔG_i, ΔG_{oe}, and ΔG_{oo} (Figure 1).[12] After fitting to this non-additive nearest-neighbor model, we found that the best fit values of ΔG_{oo} were within error of twice ΔG_{oe}, indicating that an additive nearest-neighbor model with only two parameters was appropriate, with free energies for binding to isolated sites ΔG_i, one occupied neighbor ΔG_i + ΔG_b, and two occupied neighbors ΔG_i + $2\Delta G_b$. For the six

https://dx.doi.org/10.1021/acs.biochem.0c00352
Biochemistry XXXX, XXX, XXX−XXX

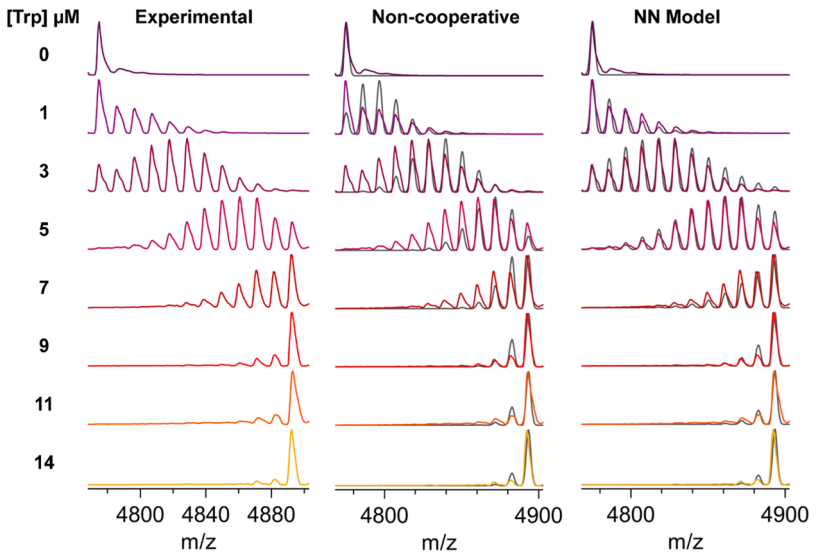

Figure 5. Population distribution of Trp_n-$TRAP_{11}$ states reveals homotropic cooperativity in Trp binding to $TRAP_{11}$. Populations of Trp_n-$TRAP_{11}$ states were fit with a binding polynomial derived from either an independent sites model or a nearest-neighbor cooperative model. The left panel shows the experimental spectra for the 19+ charge state for 1 μM $TRAP_{11}$ recorded after incubation with the indicated concentration of Trp. The middle and right panels show the experimental data were overlaid with spectra simulated using populations computed from best fits to the independent sites model and the nearest-neighbor cooperative model, respectively. The experimental population distributions are poorly described by the independent sites model, whereas the NN model generates excellent fits. Best fit parameters for the NN model were a ΔG_i of -6.86 ± 0.50 kcal mol^{-1} and a ΔG_b of -0.56 ± 0.09 kcal mol^{-1} (Table S1). Spectra were recorded at resolution of 8750 at m/z 200.

independent experiments, the best fit mean and standard deviations were $\Delta G_i = -6.86 \pm 0.50$ kcal mol^{-1} and $\Delta G_b = -0.56 \pm 0.09$ kcal mol^{-1}, yielding free energies for binding to sites with zero, one, and two occupied neighbors of -6.86 ± 0.50, -7.41 ± 0.43, and -7.93 ± 0.38 kcal mol^{-1}, respectively. These binding free energies correspond to microscopic dissociation constants for sites with zero, one, and two bound neighbors of 12.29, 4.68, and 1.82 μM, respectively. These parameters indicate an affinity somewhat weaker than that found by fitting ITC data with the NN model (−7.70, −8.74, and −8.85 kcal/mol at 40 °C, respectively)[12] but are overall consistent with the weak positive cooperativity and the adequacy of the NN model inferred from those studies.

Sources of Error. Although population distributions throughout the six independent titrations were highly reproducible, and the analysis yielded a narrow range of best fit thermodynamic parameters, we observed three sources of variability in the data. First, as mentioned above, was the difficulty in precisely defining the concentration of binding sites (i.e., TRAP) in the experiments. A challenge in quantifying TRAP concentrations is that it has a quite low extinction coefficient; it senses Trp but has no genetically encoded Trp residues. In addition, because trace amounts of Trp can significantly alter apparent concentrations, we have found it necessary to denature and refold the protein, which, though generally robust, could result in some nonproductive refolding. Indeed, difficulty in accurately quantifying TRAP binding site concentrations has resulted in some published reports treating ITC binding thermograms entirely phenomenologically, yielding no mechanistic insights.[36] Sample preparation for protein−ligand complexes for MS analysis does differ from ITC in that a series of protein samples were preincubated with varying ligand concentrations, instead of being added in a continuous fashion while allowing the solution to come to equilibrium between ligand additions; this additional handling could result in additional variation in protein concentration. The difficulty in measuring concentrations of TRAP usually resulted in titration series that seemed to saturate at somewhat lower than expected Trp concentrations. After the TRAP concentration was corrected for each series by mass balance analysis, saturation points and population distributions converged.

Second, best fit binding free energies were somewhat correlated with TRAP concentration, exhibiting increasing affinity with decreasing protein concentration (Figure S4 and Table S2). Although not definitive, this observation may be consistent with the formation of small populations of TRAP 12-mers with altered affinity for Trp. Indeed, in some of the titrations, we observed low-abundance signals corresponding to $TRAP_{12}$ (molecular weight of 101363 Da with a normalized intensity as high as 10.5% compared to that of the 11-mer); although uncommon, small populations of TRAP 12-mers have been observed in mass spectrometry experiments[41] as well as a few solution experiments,[50,51] and in crystals.[36] In addition, we observed signals corresponding to trace dimers of $TRAP_{11}$ ("double donuts"), in agreement with previous solution experiments.[52,53] However, the abundances of the signals from this species were too low for reliable quantitation, and thus, their populations were considered to be too low to be included in the analysis.

Third, upon closer analysis, we observed some charge state-dependent variability in the abundance of Trp_n-$TRAP_{11}$ signals in the nMS spectra, complicated by different relative abundances and signal-to-noise ratios for different charge states (Figure S5); separate analysis of Trp_n-$TRAP_{11}$ populations for different charge states thus resulted in slightly different best fit thermodynamic parameters (Table S4). By comparison, we observed decreased charge state dependence in AmAc data (Figure S6 and Table S5). Although this phenomenon merits further investigation, this charge state-dependent effect resulted in generally less variability than observed between replicates (free energy difference of 0.083

https://dx.doi.org/10.1021/acs.biochem.0c00352
Biochemistry XXXX, XXX, XXX−XXX

kcal mol^{-1} in EDDA, compared to a standard deviation of 0.502 kcal mol^{-1} between replicates), and positive nearest-neighbor cooperativity was required to produce reasonable fits to each data set. Overall, the titration series yielded reproducible shifts in Trp$_n$-TRAP$_{11}$ populations consistent with the nearest-neighbor cooperativity model and inconsistent with noncooperative independent binding to the 11 sites, as found previously by analysis of temperature-dependent ITC data.[12]

CONCLUSIONS

A requisite for describing an allosteric mechanism is an accurate description of the microscopic thermodynamic parameters that distinguish ligand binding events. Traditional solution-based methods for obtaining thermodynamic parameters by fitting experimentally determined observables to binding models are generally underdetermined when the number of binding sites and parameters increase, and loss of proportionality between the observable and the populations further obfuscates mechanism. A principal advantage of performing ITC experiments over a range of temperatures is that different binding modes will generally have different temperature dependencies (via their different ΔC_p), and global fitting helps to determine the proportionality between heat (i.e., ΔH) and populations (i.e., fractional binding). An additional complication with temperature-dependent measurements is that ΔC_p might not be constant over the sampled temperature range (i.e., due to shifts in the free energy landscape), which would further complicate accurate interpretation of ΔH and ΔG values. Because the mass of a macromolecule−ligand complex uniquely defines the number of bound ligands, native mass spectrometry has the potential to probe the ligand−protein partition function at a resolution that is difficult to achieve with other techniques. In the case of TRAP, direct measurement of Trp$_n$-TRAP$_{11}$ populations by nMS enabled detection and quantification of cooperativity without the need to perform titrations over a range of concentrations and temperature ranges to resolve distinct thermodynamic binding modes.[12] The results indicate that modest homotropic cooperativity indeed plays a role in regulating the cellular response to changing Trp concentrations.

The nMS approach requires the capability of resolving masses with different numbers of bound ligands, that the MS-compatible solutions not perturb the underlying thermodynamics (populations of liganded states), and that the detected ions accurately reflect populations present in solution. The modest charge state and concentration dependence of the MS data observed here and small differences with the ITC data suggest that special attention must be paid to solution and ionization conditions. Moreover, real insight requires the development and testing of accurate mechanistic models with the appropriate microscopic thermodynamic constants. The ability of nMS to probe population distributions makes it useful for modeling arbitrarily complex cooperativity models, including the classical MWC and hybrid models;[54−56] in the case of TRAP, its well-defined cyclic symmetry lattice makes straightforward and intuitive the development and application of the NN model. While not all of these requirements are likely to be met for all cases, we expect that nMS will transform how we approach the quantification and understanding of allosteric mechanisms in the plethora of important, homo-oligomeric proteins that function via cooperative ligand binding.

ASSOCIATED CONTENT

Supporting Information

The Supporting Information is available free of charge at https://pubs.acs.org/doi/10.1021/acs.biochem.0c00352.

Supplemental figures and tables (PDF)

Accession Codes

UniProt, Q9X6J6.

AUTHOR INFORMATION

Corresponding Authors

Mark P. Foster − *Department of Chemistry and Biochemistry, The Ohio State University, Columbus, Ohio 43210, United States;* orcid.org/0000-0001-9645-7491; Phone: +614-292-1377; Email: foster.281@osu.edu

Vicki H. Wysocki − *Department of Chemistry and Biochemistry and Resource for Native Mass Spectrometry Guided Structural Biology, The Ohio State University, Columbus, Ohio 43210, United States;* orcid.org/0000-0003-0495-2538; Email: wysocki.11@osu.edu

Authors

Melody L. Holmquist − *Department of Chemistry and Biochemistry, The Ohio State University, Columbus, Ohio 43210, United States;* orcid.org/0000-0003-2153-5680

Elihu C. Ihms − *VPPL, Vaccine Research Center, National Institute of Allergy and Infectious Diseases, National Institutes of Health, Frederick, Gaithersburg, Maryland 20878, United States*

Paul Gollnick − *Department of Biological Sciences, University at Buffalo, State University of New York, Buffalo, New York 14260, United States*

Complete contact information is available at: https://pubs.acs.org/10.1021/acs.biochem.0c00352

Author Contributions

P.G. provided the protein for the experiments, which was further purified by M.L.H. For *itcsimlib*, E.C.I. created scripts for fitting nMS data. M.L.H. performed all of the biochemical experiments, data analyses, and interpretation with input from M.P.F. and V.H.W. M.L.H. prepared the initial drafts of the figures and text, which were edited and finalized by M.P.F. and V.H.W. with input from all other co-authors. M.P.F., P.G., and V.H.W. secured funding to support this project and provided intellectual support for all aspects of the work. All authors have given approval to the final version of the manuscript.

Funding

This work was funded by National Institutes of Health Grants R01 GM077234 (M.P.F. and P.G.), P41 GM128577 (V.H.W.), and T32 GM086252 (M.L.H.).

Notes

The authors declare no competing financial interest.

ACKNOWLEDGMENTS

The authors thank the Gollnick lab members (especially Skylar Kelly) for protein overexpression and purification, the Wysocki lab members for sharing their MS expertise, especially Dr. Sophie Harvey and Dr. Joshua Gilbert, and the Foster lab, especially Weicheng Li, Cameron Jamshidi, and Dr. Deepak Kumar Yadav, for their input and assistance with TRAP. Access to NMR instrumentation was made possible by the Campus Chemical Instrumentation Center for their assistance with the

NMR instruments. The authors thank the Student Life Disabilities Services (SLDS) at The Ohio State University for the interpreting services provided by their American Sign Language Interpreters.

■ ABBREVIATIONS

TRAP, trp RNA binding attenuation protein; nMS, native mass spectrometry; NMR, nuclear magnetic resonance; ITC, isothermal titration calorimetry; AmAc, ammonium acetate; EDDA, ethylenediamine diacetate.

■ REFERENCES

(1) Goodsell, D. S., and Olson, A. J. (2000) Structural symmetry and protein function. *Annu. Rev. Biophys. Biomol. Struct. 29*, 105−53.
(2) Andre, I., Strauss, C. E., Kaplan, D. B., Bradley, P., and Baker, D. (2008) Emergence of symmetry in homooligomeric biological assemblies. *Proc. Natl. Acad. Sci. U. S. A. 105* (42), 16148−52.
(3) Bergendahl, L. T., and Marsh, J. A. (2017) Functional determinants of protein assembly into homomeric complexes. *Sci. Rep. 7* (1), 4932.
(4) Olivares, A. O., Baker, T. A., and Sauer, R. T. (2016) Mechanistic insights into bacterial AAA+ proteases and protein-remodelling machines. *Nat. Rev. Microbiol. 14* (1), 33−44.
(5) Skjaerven, L., Cuellar, J., Martinez, A., and Valpuesta, J. M. (2015) Dynamics, flexibility, and allostery in molecular chaperonins. *FEBS Lett. 589* (19), 2522−32.
(6) Cui, Q., and Karplus, M. (2008) Allostery and cooperativity revisited. *Protein Sci. 17* (8), 1295−307.
(7) Holt, J. M., and Ackers, G. K. (2009) The Hill coefficient: inadequate resolution of cooperativity in human hemoglobin. *Methods Enzymol. 455*, 193−212.
(8) Hilser, V. J., Wrabl, J. O., and Motlagh, H. N. (2012) Structural and energetic basis of allostery. *Annu. Rev. Biophys. 41*, 585−609.
(9) Changeux, J. P. (2012) Allostery and the Monod-Wyman-Changeux model after 50 years. *Annu. Rev. Biophys. 41*, 103−33.
(10) Gruber, R., and Horovitz, A. (2018) Unpicking allosteric mechanisms of homo-oligomeric proteins by determining their successive ligand binding constants. *Philos. Trans. R. Soc., B 373* (1749), 20170176.
(11) Wodak, S. J., Paci, E., Dokholyan, N. V., Berezovsky, I. N., Horovitz, A., Li, J., Hilser, V. J., Bahar, I., Karanicolas, J., Stock, G., Hamm, P., Stote, R. H., Eberhardt, J., Chebaro, Y., Dejaegere, A., Cecchini, M., Changeux, J. P., Bolhuis, P. G., Vreede, J., Faccioli, P., Orioli, S., Ravasio, R., Yan, L., Brito, C., Wyart, M., Gkeka, P., Rivalta, I., Palermo, G., McCammon, J. A., Panecka-Hofman, J., Wade, R. C., Di Pizio, A., Niv, M. Y., Nussinov, R., Tsai, C. J., Jang, H., Padhorny, D., Kozakov, D., and McLeish, T. (2019) Allostery in Its Many Disguises: From Theory to Applications. *Structure 27* (4), 566−578.
(12) Ihms, E. C., Kleckner, I. R., Gollnick, P., and Foster, M. P. (2017) Mechanistic Models Fit to Variable Temperature Calorimetric Data Provide Insights into Cooperativity. *Biophys. J. 112* (7), 1328−1338.
(13) Brown, A. (2009) Analysis of cooperativity by isothermal titration calorimetry. *Int. J. Mol. Sci. 10* (8), 3457−77.
(14) Vega, S., Abian, O., and Velazquez-Campoy, A. (2015) A unified framework based on the binding polynomial for characterizing biological systems by isothermal titration calorimetry. *Methods 76*, 99−115.
(15) Zhao, H., Piszczek, G., and Schuck, P. (2015) SEDPHAT–a platform for global ITC analysis and global multi-method analysis of molecular interactions. *Methods 76*, 137−148.
(16) Freiburger, L. A., Auclair, K., and Mittermaier, A. K. (2009) Elucidating protein binding mechanisms by variable-c ITC. *ChemBioChem 10* (18), 2871−3.
(17) Wiseman, T., Williston, S., Brandts, J. F., and Lin, L. N. (1989) Rapid measurement of binding constants and heats of binding using a new titration calorimeter. *Anal. Biochem. 179* (1), 131−7.
(18) Heck, A. J. (2008) Native mass spectrometry: a bridge between interactomics and structural biology. *Nat. Methods 5* (11), 927−33.
(19) Marcoux, J., and Robinson, C. V. (2013) Twenty years of gas phase structural biology. *Structure 21* (9), 1541−50.
(20) Busch, F., VanAernum, Z. L., Ju, Y., Yan, J., Gilbert, J. D., Quintyn, R. S., Bern, M., and Wysocki, V. H. (2018) Localization of Protein Complex Bound Ligands by Surface-Induced Dissociation High-Resolution Mass Spectrometry. *Anal. Chem. 90* (21), 12796−12801.
(21) Dyachenko, A., Gruber, R., Shimon, L., Horovitz, A., and Sharon, M. (2013) Allosteric mechanisms can be distinguished using structural mass spectrometry. *Proc. Natl. Acad. Sci. U. S. A. 110* (18), 7235−9.
(22) Cong, X., Liu, Y., Liu, W., Liang, X., Russell, D. H., and Laganowsky, A. (2016) Determining Membrane Protein-Lipid Binding Thermodynamics Using Native Mass Spectrometry. *J. Am. Chem. Soc. 138* (13), 4346−9.
(23) Hernandez, H., and Robinson, C. V. (2007) Determining the stoichiometry and interactions of macromolecular assemblies from mass spectrometry. *Nat. Protoc. 2* (3), 715−26.
(24) Susa, A. C., Xia, Z., Tang, H. Y. H., Tainer, J. A., and Williams, E. R. (2017) Charging of Proteins in Native Mass Spectrometry. *J. Am. Soc. Mass Spectrom. 28* (2), 332−340.
(25) Susa, A. C., Xia, Z., and Williams, E. R. (2017) Native Mass Spectrometry from Common Buffers with Salts That Mimic the Extracellular Environment. *Angew. Chem., Int. Ed. 56* (27), 7912−7915.
(26) Chait, B. T., Cadene, M., Olinares, P. D., Rout, M. P., and Shi, Y. (2016) Revealing Higher Order Protein Structure Using Mass Spectrometry. *J. Am. Soc. Mass Spectrom. 27* (6), 952−65.
(27) Ma, X., Zhou, M., and Wysocki, V. H. (2014) Surface induced dissociation yields quaternary substructure of refractory noncovalent phosphorylase B and glutamate dehydrogenase complexes. *J. Am. Soc. Mass Spectrom. 25* (3), 368−79.
(28) Zhou, M., and Wysocki, V. H. (2014) Surface induced dissociation: dissecting noncovalent protein complexes in the gas phase. *Acc. Chem. Res. 47* (4), 1010−8.
(29) Gollnick, P., Babitzke, P., Antson, A., and Yanofsky, C. (2005) Complexity in regulation of tryptophan biosynthesis in Bacillus subtilis. *Annu. Rev. Genet. 39*, 47−68.
(30) McElroy, C., Manfredo, A., Wendt, A., Gollnick, P., and Foster, M. (2002) TROSY-NMR studies of the 91 kDa TRAP protein reveal allosteric control of a gene regulatory protein by ligand-altered flexibility. *J. Mol. Biol. 323* (3), 463−73.
(31) McElroy, C. A., Manfredo, A., Gollnick, P., and Foster, M. P. (2006) Thermodynamics of tryptophan-mediated activation of the trp RNA-binding attenuation protein. *Biochemistry 45* (25), 7844−53.
(32) Kleckner, I. R., Gollnick, P., and Foster, M. P. (2012) Mechanisms of allosteric gene regulation by NMR quantification of microsecond-millisecond protein dynamics. *J. Mol. Biol. 415* (2), 372−81.
(33) Kleckner, I. R., McElroy, C. A., Kuzmic, P., Gollnick, P., and Foster, M. P. (2013) Homotropic cooperativity from the activation pathway of the allosteric ligand-responsive regulatory trp RNA-binding attenuation protein. *Biochemistry 52* (49), 8855−65.
(34) Antson, A. A., Otridge, J., Brzozowski, A. M., Dodson, E. J., Dodson, G. G., Wilson, K. S., Smith, T. M., Yang, M., Kurecki, T., and Gollnick, P. (1995) The structure of trp RNA-binding attenuation protein. *Nature 374* (6524), 693−700.
(35) Saroff, H. A., and Kiefer, J. E. (1997) Analysis of the binding of ligands to large numbers of sites: the binding of tryptophan to the 11 sites of the trp RNA-binding attenuation protein. *Anal. Biochem. 247*, 138−142.
(36) Heddle, J. G., Okajima, T., Scott, D. J., Akashi, S., Park, S. Y., and Tame, J. R. (2007) Dynamic allostery in the ring protein TRAP. *J. Mol. Biol. 371* (1), 154−67.
(37) Chen, X., Antson, A. A., Yang, M., Li, P., Baumann, C., Dodson, E. J., Dodson, G. G., and Gollnick, P. (1999) Regulatory features of the trp operon and the crystal structure of the trp RNA-binding

https://dx.doi.org/10.1021/acs.biochem.0c00352
Biochemistry XXXX, XXX, XXX−XXX

attenuation protein from Bacillus stearothermophilus. *J. Mol. Biol. 289* (4), 1003−16.
(38) Li, P. T., and Gollnick, P. (2002) Using hetero-11-mers composed of wild type and mutant subunits to study tryptophan binding to TRAP and its role in activating RNA binding. *J. Biol. Chem. 277* (38), 35567−73.
(39) Yang, M., Chen, X., Militello, K., Hoffman, R., Fernandez, B., Baumann, C., and Gollnick, P. (1997) Alanine-scanning mutagenesis of Bacillus subtilis trp RNA-binding attenuation protein (TRAP) reveals residues involved in tryptophan binding and RNA binding. *J. Mol. Biol. 270* (5), 696−710.
(40) Otridge, J., and Gollnick, P. (1993) MtrB from Bacillus subtilis binds specifically to trp leader RNA in a tryptophan-dependent manner. *Proc. Natl. Acad. Sci. U. S. A. 90* (1), 128−32.
(41) Ruotolo, B. T., Giles, K., Campuzano, I., Sandercock, A. M., Bateman, R. H., and Robinson, C. V. (2005) Evidence for macromolecular protein rings in the absence of bulk water. *Science 310* (5754), 1658−61.
(42) McCammon, M. G., Hernandez, H., Sobott, F., and Robinson, C. V. (2004) Tandem mass spectrometry defines the stoichiometry and quaternary structural arrangement of tryptophan molecules in the multiprotein complex TRAP. *J. Am. Chem. Soc. 126* (19), 5950−1.
(43) Akashi, S., Watanabe, M., Heddle, J. G., Unzai, S., Park, S. Y., and Tame, J. R. (2009) RNA and protein complexes of trp RNA-binding attenuation protein characterized by mass spectrometry. *Anal. Chem. 81* (6), 2218−26.
(44) Edelhoch, H. (1967) Spectroscopic determination of tryptophan and tyrosine in proteins. *Biochemistry 6* (7), 1948−54.
(45) VanAernum, Z. L., Gilbert, J. D., Belov, M. E., Makarov, A. A., Horning, S. R., and Wysocki, V. H. (2019) Surface-Induced Dissociation of Noncovalent Protein Complexes in an Extended Mass Range Orbitrap Mass Spectrometer. *Anal. Chem. 91* (5), 3611−3618.
(46) Marty, M. T., Baldwin, A. J., Marklund, E. G., Hochberg, G. K., Benesch, J. L., and Robinson, C. V. (2015) Bayesian deconvolution of mass and ion mobility spectra: from binary interactions to polydisperse ensembles. *Anal. Chem. 87* (8), 4370−6.
(47) Kuzmic, P. (1996) Program DYNAFIT for the analysis of enzyme kinetic data: application to HIV proteinase. *Anal. Biochem. 237* (2), 260−73.
(48) Ruotolo, B. T., Benesch, J. L., Sandercock, A. M., Hyung, S. J., and Robinson, C. V. (2008) Ion mobility-mass spectrometry analysis of large protein complexes. *Nat. Protoc. 3* (7), 1139−52.
(49) Konermann, L., Metwally, H., Duez, Q., and Peters, I. (2019) Charging and supercharging of proteins for mass spectrometry: recent insights into the mechanisms of electrospray ionization. *Analyst 144* (21), 6157−6171.
(50) Bayfield, O. W., Chen, C. S., Patterson, A. R., Luan, W., Smits, C., Gollnick, P., and Antson, A. A. (2012) Trp RNA-binding attenuation protein: modifying symmetry and stability of a circular oligomer. *PLoS One 7* (9), No. e44309.
(51) Heddle, J. G., Yokoyama, T., Yamashita, I., Park, S. Y., and Tame, J. R. (2006) Rounding up: Engineering 12-membered rings from the cyclic 11-mer TRAP. *Structure 14* (5), 925−33.
(52) Ihms, E. C., Zhou, M., Zhang, Y., Kleckner, I. R., McElroy, C. A., Wysocki, V. H., Gollnick, P., and Foster, M. P. (2014) Gene regulation by substoichiometric heterocomplex formation of undecameric TRAP and trimeric anti-TRAP. *Proc. Natl. Acad. Sci. U. S. A. 111* (9), 3442−7.
(53) Snyder, D., Lary, J., Chen, Y., Gollnick, P., and Cole, J. L. (2004) Interaction of the trp RNA-binding attenuation protein (TRAP) with anti-TRAP. *J. Mol. Biol. 338* (4), 669−82.
(54) Tsai, C. J., and Nussinov, R. (2014) A unified view of "how allostery works. *PLoS Comput. Biol. 10* (2), No. e1003394.
(55) Motlagh, H. N., Wrabl, J. O., Li, J., and Hilser, V. J. (2014) The ensemble nature of allostery. *Nature 508* (7496), 331−9.
(56) Gruber, R., Mondal, T., and Horovitz, A. (2019) GroEL Allostery Illuminated by a Relationship between the Hill Coefficient and the MWC Model. *Biophys. J. 117* (10), 1915−1921.

https://dx.doi.org/10.1021/acs.biochem.0c00352
Biochemistry XXXX, XXX, XXX−XXX